Catalysis Today 147 (2009) 287–299

Contents lists available at ScienceDirect

Catalysis Today

journal homepage: www.elsevier.com/locate/cattod

The role of mechanically induced defects in carbon nanotubes to modify the properties of electrodes for PEM fuel cell☆

G. Centi [a], M. Gangeri [a], M. Fiorello [a], S. Perathoner [a,*], J. Amadou [b], D. Bégin [b], M.J. Ledoux [b], C. Pham-Huu [b], M.E. Schuster [c], D.S. Su [c], J.-P. Tessonnier [c], R. Schlögl [c]

[a] Dept. of Industrial Chemistry and Materials Engineering, University of Messina, Salita Sperone 31, 98166 Messina, Italy
[b] Lab. Des Matériaux, Surface at Procédés pour la Catalyse, CNRS &ULP, Strasbourg, France
[c] Fritz Haber Institut der M.P.G., Berlin, Germany

ARTICLE INFO

Article history:
Available online 14 August 2009

Keywords:
CNT
Pt
Defect
Electrode
PEM fuel cell

ABSTRACT

The characteristics and reactivity of two anodes based on Pt supported on carbon nanotubes (CNTs) without or with defects induced by ball-milling are studied by SEM, TEM, cyclic voltammetry (CV) and single-cell measurements using a flow of pure H_2 or containing 50 ppm CO. It is evidenced that the presence of defects influences several properties and not only the dispersion of Pt particles. Therefore, the performances cannot be correlated neither with the geometrical surface area of Pt particles, neither with the electrochemical active surface area determined from CV tests. The presence of defects, enhancing the amount of surface functional groups on CNT, influences various aspects: (i) the efficiency of three-phase boundary and thus the transport of protons to or from the active metal particles, (ii) the resistance of electron transfer and (iii) the tolerance of the catalyst to CO poisoning. The latter is attributed to carbon functional groups in close contact with very small Pt particles favoring the reactivation of Pt sites poisoned by CO.

1. Introduction

There is a growing interest on the use of nanostructured carbon materials (carbon nanotubes, -fibres, etc.) to improve the performances of PEM fuel cells, as specifically reviewed recently [1] and discussed in part in other review papers [2–5]. The main motivations can be summarized as follows:

(i) The unique structure and electrical properties of carbon nanotubes (CNT) and other 1D-type nanostructured carbon materials which provide a high electrical conductivity and a specific interaction between catalyst metal nanoparticles and the carbon support, i.e. between the delocalized π electrons of CNTs and Pt *d*-electrons. These aspects are relevant to determine aspects (a) a faster rate of transfer of electrons during operations from the metal to the conducting substrate, which reduce the metal nanoparticle charge and improve current densities and (b) a better dispersion and stabilization of metal nanoparticles with respect to sintering.

(ii) Carbon nanotubes or related materials have typically few impurities, while carbon black (the most common used carbon material for preparing electrodes for fuel cells; an example is Vulcan XC-72) contains significant quantities of organosulfur impurities, which can poison Pt metal, although their presence is necessary for a good stability of the performances.

(iii) Carbon nanotubes or related materials have a higher accessible area in contact with the proton-transport membrane, while Pt nanoparticles present in micropores of carbon black have a poor contact, with a consequent lower activity due to a poor triple-phase boundary (electron transported by the conductive carbon, the gas reactant and the proton transported to or from the proton-conductive membrane).

(iv) Hierarchically organized structures can be prepared, for example by growing carbon nanotubes (CNTs) on a carbon cloth substrate (CC) which is formed by carbon fibres having several micron diameter with respect to the nanometric size of the CNT. These CNT/CC composite materials thus provide the opportunity for a better design to optimize mass/electron transport [6,7], resulting in higher cell performances. Similar, highly interesting is the possibility to prepare oriented nanostructures (an array of aligned nanotubes) also to optimize the catalyst/membrane/gas reactant/conductive support interaction [5].

☆ Work realized in the frame of ELCASS (European Laboratory of Catalysis and Surface Science).

* Corresponding author. Tel.: +39 090 6765609; fax: +39 090 391518.
E-mail address: perathon@unime.it (S. Perathoner).

0920-5861/$ – see front matter © 2009 Elsevier B.V. All rights reserved.
doi:10.1016/j.cattod.2009.07.080

A number of studies have reported the superior performances of carbon nanotubes based electrodes for PEM fuel cells, but we may observed that in general the interpretation is often only related to the possibility of a better dispersion of metal particles. For example, Saha et al. [8] studied 3D composite electrodes consisting of Pt nanoparticles supported on nitrogen-doped carbon nanotubes (CNx) grown directly on the carbon paper. The superior performances as electrode in PEM fuel cells were related only to the possibility of a better dispersion of Pt nanoparticles, i.e. smaller size (around 2–3 nm) and higher electrochemical Pt surface area. Cui et al. [9], studying PtRu catalysts supported on carbon nanotubes for methanol electro-oxidation, also concluded that the improved properties with respect to carbon black support is due to the formation of uniformly dispersed Pt–Ru particles with small average size (2.7 nm). Maiyalagan [10] analyzing the electrocatalytic activity in methanol oxidation of Pt supported on N-doped carbon nanotubes also concluded that the role of carbon nanotubes is to provide a better dispersion for Pt particles. Kim et al. [11], comparing the behaviour of Pt deposited on carbon nanotubes and carbon black, concluded that smaller and more uniform metal particles are present on carbon nanotubes and to this effect could be ascribed the higher performances in PEM fuel cells. Tuseeva et al. [12] reported that in methanol oxidation using Pt–Ru based electrocatalysts the current values per unit true surface area do not depend on the support nature (carbon nanotubes and standard carbon black Vulcan XC-72), provided the catalyst loading is equal and the particle size is similar.

On the other hand, other authors instead concluded that carbon nanotubes do not show performances different from those of conventional electrocatalysts. For example, Verde et al. [13] concluded that Pt–Ru on multi-wall carbon nanotubes (MWCNTs) show performances comparable with traditional catalyst in PEM fuel cells.

Single-wall (SWNT), double-wall (DWNT) and multi-wall (MWNT) could be prepared and were used to prepare electrode for PEM fuel cells, but often the results were contrasting. For example, Wu and Xu [14] reported that catalysts based on Pt supported on SWNT show better performances in methanol oxidation than on MWNT, due to higher utilization of Pt metal. Li et al. [15] reported instead that DWNT is preferable over single- and multi-wall carbon nanotubes. Other authors instead found preferable the use of MWNT based materials [1]. Not unique and definite conclusions also could be derived from literature data regarding the role of other carbon nanostructure, such as bamboo-structured MWNT [16] or herringbone carbon nanofibres (CNFs), in which the axis of the graphite planes is at an angle with respect to the main axis of nanotubes.

The issue is that often are indicated as carbon nanotubes materials, which have quite different characteristics. To limit the discussion to MWNT case, it is known that quite different characteristics of the CNT could be obtained depending on the preparation, in terms of not only nanotubes size and wall thickness, but also amount and nature of defects. Their presence influence the conductivity of CNT, the stability (the corrosion of carbon material always initiates at defect sites [17]) during operations, and the dispersion of Pt, although literature information are limited. However, it was reported recently [18] that pentagon defects introduced in a bamboo-shaped carbon nanotube support for PtRu nanoparticles allows to prepare highly active anode for direct methanol fuel cells. Such an enhancement was ascribed to an enhanced interaction of the introduced pentagon defects with Pt–Ru particles, which promotes a high loading and well dispersion of Pt–Ru catalysts and the charge transfer from Pt–Ru to the tubes. A recent theoretical study [19] has analyzed the adhesion of various sizes of Pt clusters on carbon nanotubes with and without the presence of point defect. The calculations showed that the binding energies of Pt clusters on the defect-free CNTs are more than 2.0 eV. However, the binding energies are increased more than three times on the point defective CNTs. The dramatic increase of the binding energy has been explained by the partial delocalization of states and deformation charge density. The stronger orbital hybridization between the Pt atom and the carbon atom shows larger charge transfers on the defective CNTs than on the defect-free CNTs, which allows the strong interaction between Pt clusters and CNTs.

On the other hand, Yoo et al. [20], studying the support effect (CNTs with and without defects, carbon black, and fishbone-type CNTs) for direct methanol fuel cell (DMFC), showed that Pt–Ru/defect-free CNTs afforded the highest catalytic activity of methanol oxidation in rotating disk electrode experiments and the highest performance as the anode catalysts in DMFC single-cell tests with the one-half platinum loading compared to Pt–Ru/Vulcan XC-72R.

Defects are usually introduced in CNT by oxidation pretreatment of the CNT using nitric acid, H_2O_2 or other reactants. The treatment is necessary to obtain a good dispersion of the metal particles. These methods, in fact, create different surface function groups (lactone, pyran, carboxylic, anhydride, quinone, phenol, furan), although several of these groups have a low thermal stability. It is known that the type of pretreatment influences the dispersion and electrocatalytic activity [21], but often results are only phenomenological. In addition, other type of defects not associated to oxidation treatment could be present in CNT, such as vacancies, vacancy-related defects or nonhexagonal carbon rings [22]. These topological defects may occur in the as-grown nanotubes, or they can be generated by several methods like chemical treatment, mechanical or irradiation treatments.

The problem of the role of defect in carbon nanotubes used to prepare electrocatalysts for PEM fuel cell is thus a relevant topic for the development of improved electrodes, but detailed studies on this aspect are still limited, due also to the complexity of the problem. The aim of this work is to contribute to this aspect by analyzing the characteristics and electrochemical performances of Pt nanoparticles deposited with the same methodology on carbon nanotubes without and with the presence of defects induced mechanically by ball-milling, a procedure often used to shorten and open multi-wall carbon nanotubes produced by chemical vapour deposition (CVD) method [23]. The performances using pure and CO-containing H_2 were evaluated, because it has been reported that the carbon substrate affects the resistance to deactivation by CO [24,25] and thus the defects in CNT could play a role to promote CO-tolerant electrodes for PEM fuel cells.

2. Experimental

2.1. Preparation of the electrocatalysts

MWCNT have been prepared by chemical vapour deposition (CVD). The support used for the preparation of the catalyst for carbon nanotubes growth was a high surface area γ-Al_2O_3 (CK 300B from Ketjen with a specific surface area of 220 m^2/g), which was mainly composed of a mesoporous network. The alumina support was crushed and sieved and the fraction of 40–80 μm was retained for catalyst preparation. The catalyst was prepared by an incipient wetness impregnation method using an aqueous solution of $Fe(NO_3)_3{\cdot}9H_2O$, with a theoretical Fe concentration fixed at 20 wt.%. The iron loading was measured by means of the ICP-MS method and was amounted to 19 wt.% which is relatively close to the theoretical one. The wet solid was dried at 100 °C and then calcined in air at 450 °C for 2 h in order to obtain the oxidized form of the catalyst precursor; the reduction was performed for 1 h under H_2 flow of 100 mL/min at 400 °C. Initially, the experimental conditions of the CVD synthesis have been optimized in order to

improve the carbon nanotube yield and purity. In the optimized conditions, one gram of iron allows the production of 15 g of MWNTs per hour (1500 wt.% yield) with a purity up to 90%, with a total flow rate of 2 L/min (C_2H_6/H_2, 60/40 vol.%) at 700 °C for 3 h.

The purification of these CNT from the presence of alumina and iron was made using standard purification methods: an acidic treatment was used in order to remove iron particles followed by a basic treatment in order to remove the alumina support. The acid used was nitric acid under reflux at 120 °C for 24 h, while the base was sodium hydroxide, also used under reflux at 120 °C for 24 h.

After purification, the as-synthesized CNT have been treated by a ball-milling (BM) procedure, which, as shown in the introduction, is a method often used to break-down and open the CNTs, because the CVD method produces large amounts of close-end nanotubes. BM treatments have been done in a planetary ball-mill (*Fritsch Pulverisette 5*) using 15 steel (with ~4.5 at.% C and 1.5% Cr) balls with a diameter of ~1 cm and steel (with ~6.7 at.% C and 12 at.% Cr) vials. Milling experiments were carried out without interruption for 90 min under an inert atmosphere (argon) and the rotational speed of the central plate was 360 rpm. The sample will be indicated CNT_d hereinafter, because the BM method produces large amounts of defects.

MWCNT supplied by Applied Science Ltd. (US) in a purified form (Pyrograph III, grade PR24-XT) were utilized as the second sample without mechanically induced defects (CNT_{nd}). In fact, in the former sample, prior to BA treatment, the deposition of Pt do not result to homogeneous and well-dispersed samples and was thus necessary to use slightly larger CNTs, which allowed preparing much more comparable materials. On the other hand, BA procedure on Applied Science CNTs was much less effective in creating mechanically induced defects, due to their higher hardness. Note, that no oxidative pretreatment has been made prior to deposit the noble metal for both CNTs. This procedure is often used to enhance the dispersion of supported metals, but in this case could mask the role of defects due to the mechanical treatment.

Pt (10 wt.%) was deposited by incipient wetness impregnation of a C_2H_5OH/H_2O (20:80%) solution with H_2PtCl_6 (Strem Chemicals). The mixture was allowed to dry at room temperature for 12 h and then oven-dried at 100 °C for 2 h. The dry CNT containing the active phase precursor were slowly heated at 350 °C under air for 2 h and finally reduced at 400 °C under H_2 flow for 2 h. This reduction temperature was used (i) to have all the Pt particles in the metallic state, and (ii) to avoid later sintering during the electrocatalytic tests, e.g. have more stable electrocatalysts.

The Pt/CNT materials prepared in this way were then used to prepare the MEAs (membrane and electrodes assembly) for the electrochemical measurements as anode in lab-scale (about 1 cm^2) PEM fuel cells. A commercial 20 wt.% Pt/Vulcan XC-72 on carbon cloth electrode (E-TEK Inc.) was used for the cathode. The anodes were prepared depositing on E-TEK ELAT carbon cloth a suspension containing a 10 wt. % Nafion solution and the different electrocatalysts based on Pt supported on CNT. Commercial 20 wt.% Pt and Pt–Ru (1:1) on carbon black catalysts from E-TEK were used as reference. The final amount of metal active phase in all the electrodes constituting the MEA is about 0.5 mg/cm^2. Before being used in manufacturing MEAs, the polymer electrolyte membrane, Nafion® 115 (DuPont Chemical), was cleaned by immersing in 3% H_2O_2 for 1 h at 80 °C to remove organic impurities and then in 0.5 M H_2SO_4 for 1 h at 80 °C; the H_2SO_4 was removed by repeated washing in boiling distilled water. The MEAs with a geometric area of 1 cm^2 were assembled by hot-pressing.

2.2. Characterization

The morphology and size of the Pt nanoparticles dispersed on the carbon nanotubes were characterized by transmission electron microscope (TEM, Philips CM200 LaB6). High-resolution images were acquired on the TEM-FEG (Manfred Schuster). Lattice spacings were determined from Fourier Transform of selected areas of the images. The localization of Pt particles inside and outside the CNT was analyzed by tilting which the samples over a sequence of angles.

Scanning electron micrographs were made using a FESEM (field emission scanning electron microscope) Hitachi S4800 equipped with EDX.

The distribution (in terms of nr. of particles) of Pt particle in Pt/CNT_{nd} and Pt/CNT_d samples was made by particle analysis using TEM images. Based on the observed distribution of Pt particles, it is possible to determine the geometrical surface area (GSA) of Pt, using on the following equation assuming round-shaped geometry for all particles [26]:

$$GSA = \sum_i \omega_i \frac{6000}{\delta d_i} \quad (1)$$

where ω_i is the fraction of particles with mean diameter d_i and δ is the density of Pt (21.4 g cm^{-3}).

2.3. Electrochemical measurements

Cyclic voltammetry was used to study the electrochemical properties of the catalyst by a thin-film electrode technique [25]. Briefly, a glassy carbon disk was used as the substrate, on which 5 μL of a paste of the catalyst was applied. The catalysts were attached to the glassy carbon disk according to the following procedure: an amount of the catalyst powder was dispersed ultrasonically in the water solution to obtain a homogeneous black suspension solution with 2 mg mL^{-1} Pt/CNT. The suspension was pipetted onto the surface of a glassy carbon disk electrode. After the paste dried, a drop of 5 wt.%. Nafion in alcohol solution was spread on the catalyst and allowed to dry. A recast ionomer thin-film covering with the catalyst was thus obtained. Each electrode contained about 0.1–0.2 mg cm^{-2} of the catalyst.

A standard electrochemical cell, connected to an Autolab PGSTAT30 potentiostat/galvanostat, was used for the measurements in 0.5 M H_2SO_4 solution at room temperature. The glassy carbon disk covered with the catalyst was used as working electrode. The cyclic voltammograms were generally recorded at a scan rate of 50 mV/s in the potential range from −0.22 to 1.2 V vs. Ag/AgCl (E^o = 0.22 V). The four cycle of each measurement was used for the evaluation, in order to remove eventual impurities.

The electrochemical cell tests in hydrogen oxidation of the MEA were carried out in a homemade PEM fuel cell (geometric area 1 cm^2), working at r.t. (20 °C) and atmospheric pressure, connected by a platinum wire to a potentiostat/galvanostat (Autolab PGSTAT30). The pure H_2 and O_2 feed arriving from cylinders (purity > 99.9%) and regulated through flow meters, were saturated with H_2O at r.t. prior to be send to the anode and cathode sides of the fuel cell, respectively. The polarization curves and power density curves were recorded after stability of the performances, usually after 30 min. Each point of the polarization curves represents a steady-state performance achieved after at least 5 min of continuous operation at a given voltage.

The electrochemical cell tests in the presence of CO were made in the same apparatus and reaction conditions, but feeding 50 ppm CO in H_2 at the anode side, using a pre-calibrated mixture stored in a cylinder.

Note that to avoid the presence of relevant mass-transfer limitations and the limiting effect of cathode, the tests were made at a lower temperature (20 °C) with respect to the usual temperature (about 80 °C) utilized in PEM single-cell experiments. The maximum power densities are clearly lower than those which

can be obtained at 80 °C, but the purpose of this work was not to demonstrate whether CNT could be better or not to carbon black, but to analyze instead the role of mechanically induced defects in the modifications of the properties of supported Pt nanoparticles. Therefore, reaction conditions to minimize other effects have been chosen.

The estimation of the electrochemical active surface area (EAS) can be made by cyclic voltammetry (CV) experiments in acid solution (Ar-saturated 0.5 M H_2SO_4 aqueous solution at room temperature). When the electrode potential is ramped linearly to a more positive potential (with respect to RHE) adsorbed hydrogen on Pt is oxidized to protons and electrons approximately in the 0–0.5 V range:

$$Pt{-}H_{ads} \rightleftharpoons Pt + H^+ + e^- \quad (2)$$

while at higher potential Pt is first converted to Pt–OH and then to oxide. By decreasing the potential, the oxide is first reduced (approximately in the 0.5–1.0 V range) and at lower potential Pt–H_{ads} reforms. Due to the presence of different exposed crystalline faces for Pt particles, multiple peaks of direct and inverse reaction (2) are usually observed. The EAS can be calculated from the CV curve, by calculation of the Coulombic charge for the hydrogen adsorption and desorption (Q_H) [26–28]. The value of Q_H (mC cm^{-2}) is the mean value between the amounts of charge transfer during the electroadsorption and desorption of H_2 on Pt sites [29], corrected by the contribution of double layer charge and eventually the support contribution. The EAS can be then calculated from the following equation:

$$EAS = \frac{Q_H}{[Pt]0.21} \quad (3)$$

where [Pt] represents the platinum loading (mg cm^{-2}) in the electrode, and 0.21 represent the charge required to oxidize a monolayer of H_2 on bright Pt [30].

3. Results and discussion

3.1. Physicochemical characterization

TEM image of the CNT_{nd} support are presented in Fig. 1a. The carbon nanotubes are curved, twisted together and display an average external diameter ranging between 60 and 100 nm and length up to several hundred micrometers. The tubes are open on both ends owing to their relatively large diameter, which prevents the formation of caps on the tube tip. Fig. 1b shows TEM images of CNT_d before BM. The mean external diameter is smaller, in the 5–15 nm range, but some larger tubes of 25 nm and above diameter are present. The mean length of CNT is over 100 μm and the majority of CNT have closed tips. Most of the CNTs are straight and not entangled.

Fig. 2 shows HRTEM images of the ends of the ball-milled CNT_d. For most of the nanotubes, the angle between tube axis and the fracture on the surface is ≤90° (Fig. 2a). Furthermore, it is evident, after BM treatment, the presence of a high number of defective sites (Fig. 2b). The main events in the process are collision and friction between stainless steel balls and the nanotubes. Calculations of the elastic properties of CNT predicted that they are extremely rigid in the axial direction but most likely to be distorted perpendicularly [31]. During ball milling, frequent collisions and the high velocity of the steel balls cause strong impacts on the nanotubes. If the collision energy is high enough, the cylinder structure of the CNT will be cracked at the sites impacted and the graphene layers ruptured completely. Thus short nanotubes with open ends can be formed. Milled nanotubes are prone to break at the sites of structural defects, such as bends, thus causing that the majority of milled CNT to be straight. Besides, if the intensity of collisions is not high enough to cause nanotube cleavage, they will make more defects on the tube walls.

The TEM micrographs of Pt/CNT_{nd} and Pt/CNT_d samples (loading of 10% in weight of Pt) are shown in Figs. 3 and 4, respectively. The same procedure of deposition of Pt has been used for the preparation of the two samples, and no oxidative pretreatment of the CNT has been made prior the loading with Pt. In Figs. 3 and 4, pictures a–c were TEM images at different resolution to evidences the distribution of the Pt nanoparticles within the nanotubes, while pictures d–f were HRTEM images at higher resolution to evidence the characteristics and size of the Pt nanoparticles.

In Pt/CNT_{nd} (Fig. 3), different type of Pt particles could be detected. Quite small Pt particles, below 1.5–2.0 nm, which are homogeneously distributed in all CNTs. They are present both on the inner and outer surface of CNT (see inset in Fig. 3d), but predominantly on the outer surface. These particles are round-shaped. A second type of particles, also round-shaped, has a larger diameter, within about the 2–5 nm range, and is present predominantly within the CNT, e.g. in the nanotubes. It may be observed, however, that the loading of these Pt nanoparticles is quite different from one CNT to the other (see Fig. 3b and c), even if there is not visible difference in the characteristics of the CNT, as appeared from TEM images. The preparation again of the sample lead to similar results which thus indicates that the inhomogeneous loading was related to the characteristics of the single CNTs, more than to an effect of the preparation. The third type of Pt

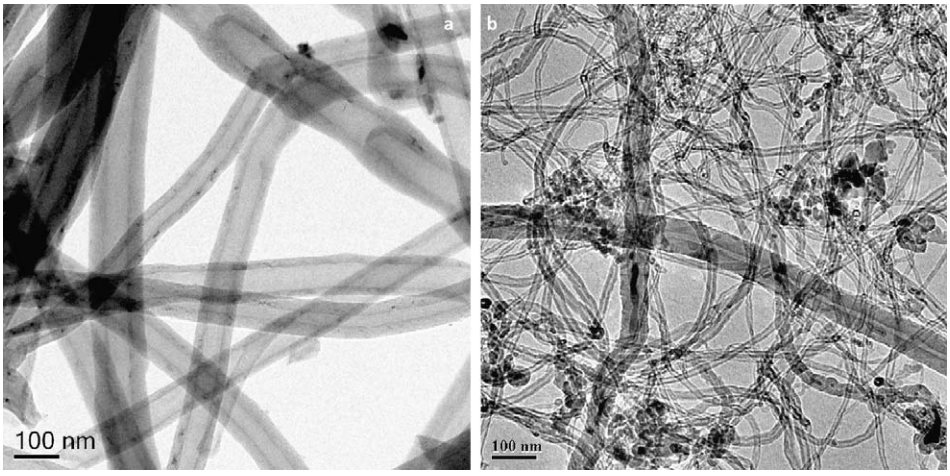

Fig. 1. Transmission electron microscopy (TEM) images of CNT_{nd} (a) and CNT_d before ball-milling (BM) (b).

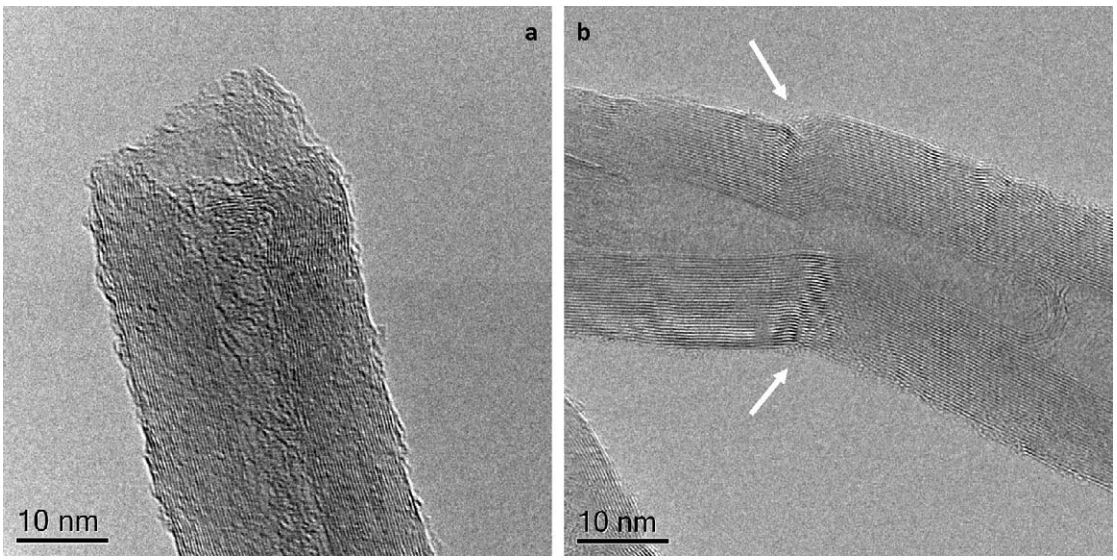

Fig. 2. High-resolution transmission electron microscopy (HRTEM) images of CNT_d after BM showing the opening of the tip (a) and the presence of defect sites indicated by arrows (b).

particle is bigger, elongated and faceted. These particles are 9–16 nm long and 7–11 nm large. They are essentially located within the CNTs and present only in some of the CNTs. An HRTEM image of these particles is shown in Fig. 5a. Lattice distances, determined from Fourier Transform of selected areas, were found to be 2.23 ± 0.03 and 1.96 ± 0.02 nm, attributed to Pt(1 1 1) and Pt(2 0 0), respectively. To note that X-ray diffraction analysis, due to small particle size and the presence of Pt particles with various shapes (see TEM images), do not gives reliable indications on these crystallographic aspects. The different location of the particles, as indicated by TEM images in which the samples were tilted over a sequence of angles, is due reasonably to the different characteristics (and presence of defects) of the inner and outer surface of the CNT. The inner surface is less defective and more graphitic, as confirmed by TEM images. Therefore, a faster mobility and coalescence of Pt particles is expected.

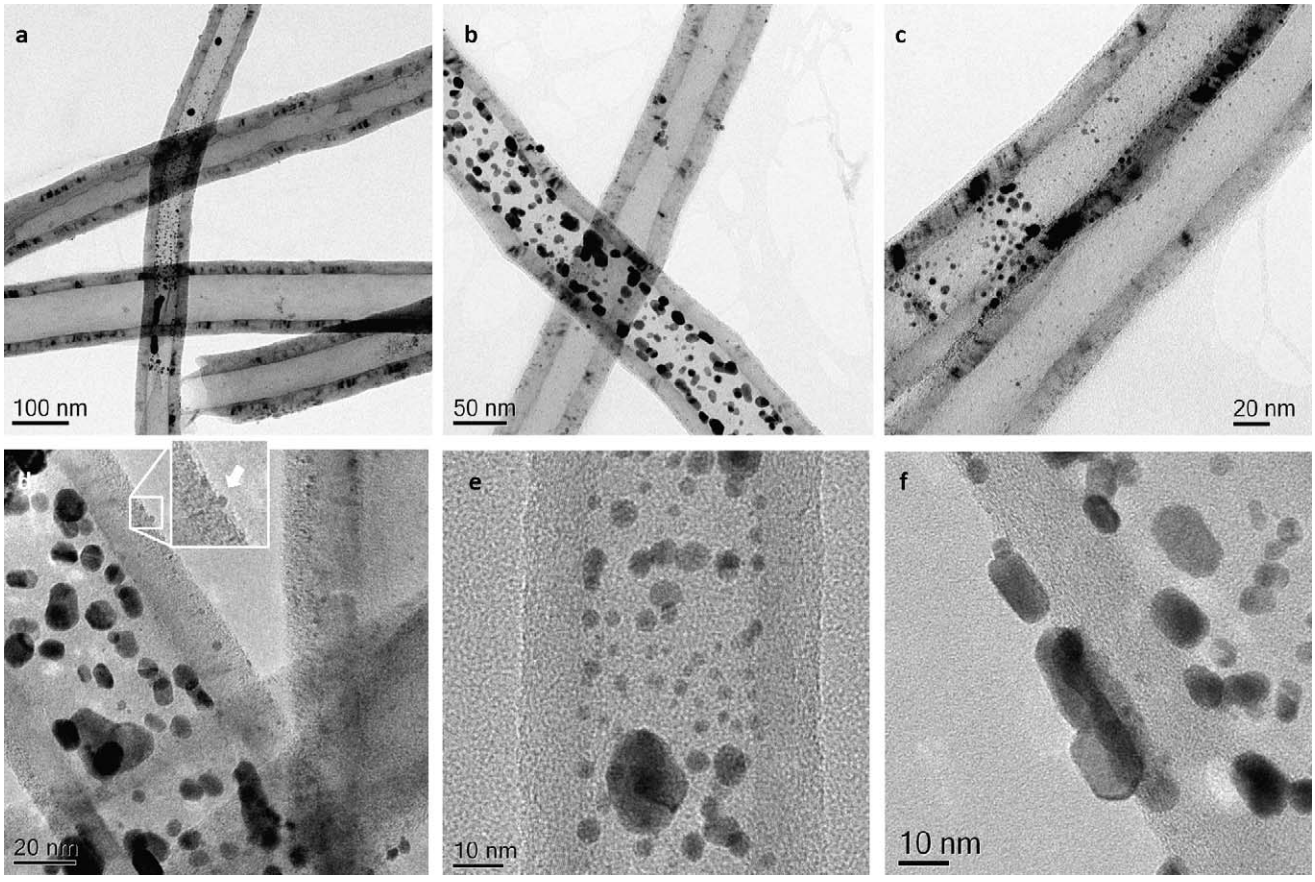

Fig. 3. TEM (a–c) and HRTEM (d–f) images of CNT_{nd}.

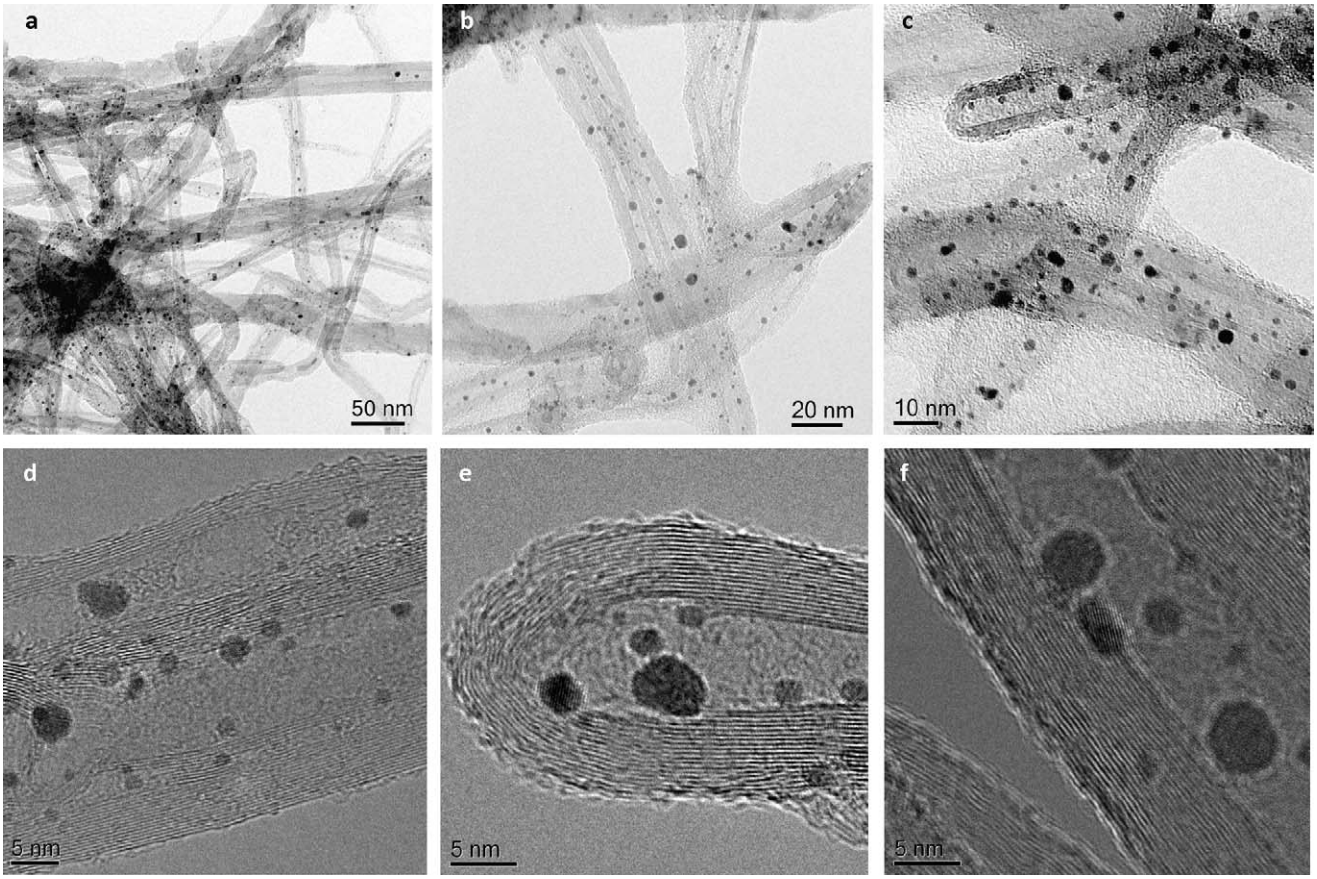

Fig. 4. TEM (a–c) and HRTEM (d–f) images of CNT_d.

In Pt/CNT_d (Fig. 4), a more homogeneous distribution of Pt particles within all the nanotubes could be observed. Together with very small Pt nanoparticles (below 1.0–1.5 nm) located on the inner (predominantly) and outer surface of carbon nanotubes, larger round-shaped particles with diameter in the 2–5 nm range (with few larger in the 5.5–6.6 nm range) were observed. Fig. 5b shows a HRTEM image of these particles. Lattice spacing was determined from Fourier transform of selected areas of the images. The measured distances were typically 1.95 ± 0.04 and 2.26 ± 0.02 nm, respectively attributed to Pt(2 0 0) and Pt(1 1 1). Fig. 5c also shows a HRTEM image of one of the small Pt nanoparticles located on the outer CNT surface (indicated with an arrow, diameter about 0.5 nm) which appears to be partially incorporated within the carbon nanosheets.

The distribution (in terms of nr. of particles) of Pt particle in Pt/CNT_{nd} and Pt/CNT_d samples is reported in Fig. 6. The average size of Pt particles in Pt/CNT_d is 1.4 nm, while Pt/CNT_{nd} shows a bimodal distribution, centred 1 and 4.5 nm, respectively. The average size of Pt particles in Pt/CNT_{nd} is 3.0 nm. For reference, the mean size of Pt particles in Pt/Vulcan XC-72 electrocatalysts was found to be about 3.6 nm [26]. A similar value (about 3.2 nm) was found be us for the E-TEK Pt/Vulcan XC-72 sample used by us as reference for electrochemical experiments. The average size of Pt particles determined from the Pt(1 1 1) peak of the X-ray diffraction patterns using the Debye-Scherrer equation was found to be consistent with the average size estimated from TEM measurements.

With the observed distribution of Pt particles, it is possible to determine the geometrical surface area (GSA) of Pt using Eq. (1) reported in the Section 2. The results are summarized in Table 1 and evidences that the GSA for Pt/CNT_d is about 25% higher than that of Pt/CNT_{nd}, due to the higher amount of small particles. For reference, the geometrical surface area estimated based on only the average particle size is reported. For Pt/CNT_{nd}, where a bimodal distribution is present, the estimation using only the mean particle size leads to a significant underestimation of the GSA.

It should be also noted that the approximation of round-shaped geometry used to estimate GSA is reasonable, because TEM images evidence a different geometry only for particles above about 6 nm, but which give a minimal contribution to overall surface area, being present in a much lower number with respect to the others (Fig. 6).

3.2. Electrochemical active surface area

GSA is an indication of the total available surface area, and depends on the dispersion of Pt on the support. However, GSA do not provide an estimation of the electrochemical active surface area, because part of the Pt particles may be inactive, due to a poor contact with the carbon conductive substrate, or because part of the surface area is not accessible to the gas reactants. The estimation of the electrochemical active surface area (EAS) can be made by cyclic voltammetry (CV) experiments (see Section 2). The CV curves for Pt/CNT_d and Pt/CNT_{nd} are reported in Fig. 7a and b, respectively. As reference, the CV of E-TEK Pt/Vulcan XC-72 sample is also shown. Fig. 7b also reports the general attribution of the different regions in CV curves, to help the discussion.

A first observation is the apparent quite different overall shape of CV curves between Pt/CNT_d (Fig. 7a, quite similar to Pt/Vulcan XC-72) and Pt/CNT_{nd} (Fig. 7b). However, the problem arises from the fact that there is oxidation of the carbon substrate (CNT_d and Vulcan XC-72, particularly in CNT_d, while the effect is minimal in CNT_{nd}. Maruyama and Abe [32] have investigated by cyclic

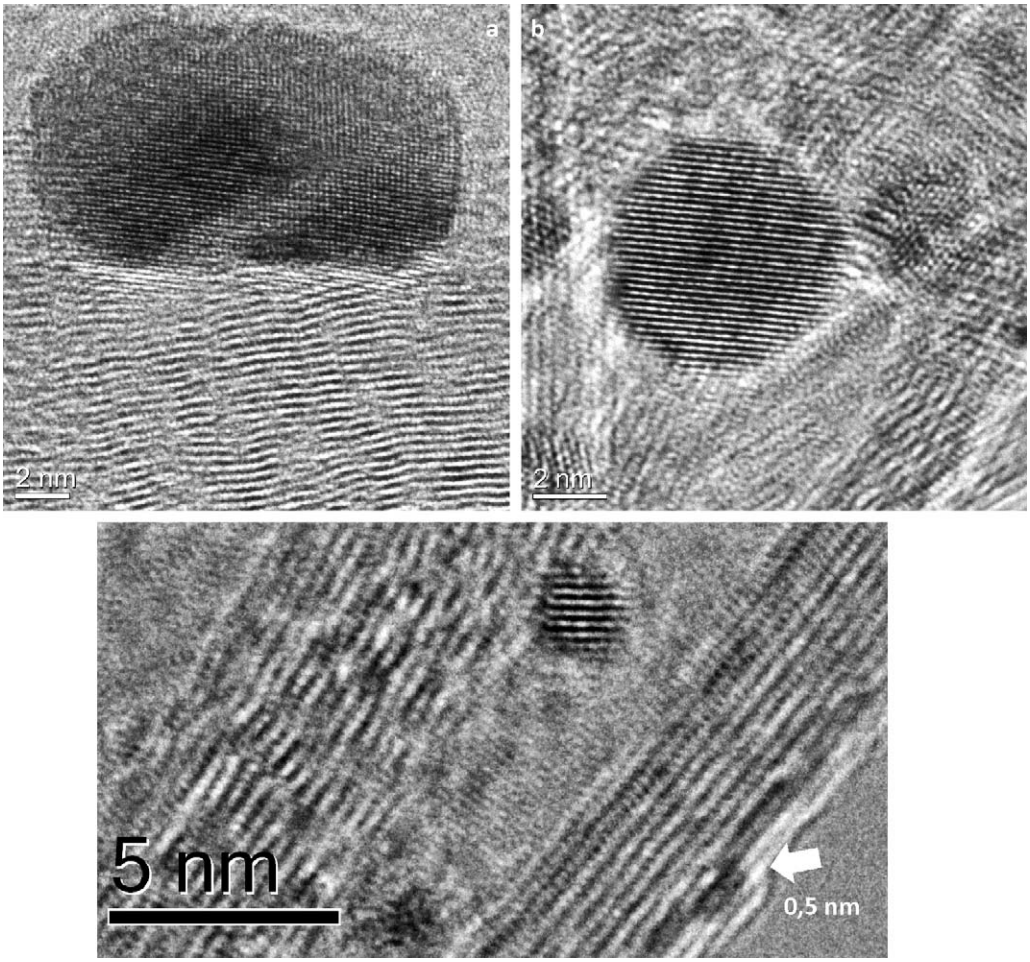

Fig. 5. HRTEM images of Pt particles in CNT_{nd} (a) and CNT_d (b and c). See text for details.

voltammetry the behaviour of glassy carbon (GC) electrodes, where the surface was electrochemically oxidized to impart hydrophilicity. The surface oxidation generated oxygen-containing surface functional groups, especially quinone-like ones. Increasing the degree of surface oxidation, the current in both anodic and cathodic scans increased and a broad peak centred at around 0.35 V (with respect to SCE) both in the anodic and cathodic CV sides were observed. These peaks were caused by the redox reaction of quinone-like functional groups on the GC surface:

$$Qu + 2H^+ + 2e^- \rightleftharpoons QuH_2 \quad (4)$$

The different shape in CV curves of Pt/CNT_d and Pt/CNT_{nd} is thus related to the higher degree of surface defects of the former and thus the overlap of the CV contribution of the support to that of Pt. It is not possible to simply subtract the CV curve for the support alone, due to presence of hydrogen spillover from the metal to carbon support and the influence of the supported noble metals on the reactivity of surface functional groups of carbon, but only report an estimated contribution of the carbon nanotube support to the CV curve of Pt/CNT_d (see Fig. 7a).

A second observation regards the shift to lower potential of the Pt–O reduction, from about 0.55 V in Pt/CNT_{nd} to 0.35 V in Pt/CNT_d. Taking into consideration the CV contribution mentioned above for redox reaction of quinone-like functional groups, the position of

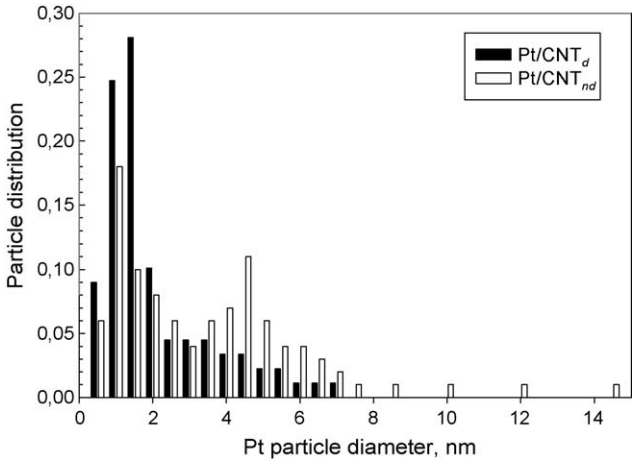

Fig. 6. Distribution of Pt particle diameter in CNT_{nd} and CNT_d determined from TEM measurements.

Table 1
Electrochemical active surface area (EAS) determined from CV experiments, geometrical surface area (GSA) estimated on the basis of the mean diameter of Pt particles or of the size distribution shown in Fig. 6, and mean value of the ratio of the EDX peak intensities of F and Pt (see Fig. 8d).

Sample	EAS ($m^2\ g^{-1}$)	GSA ($m^2\ g^{-1}$)		F/Pt
		Based on mean diameter	Based on size distribution	
Pt/CNT_d	163.3	200.3	207.6	1.3
Pt/CNT_{nd}	114.3	93.5	151.8	0.8

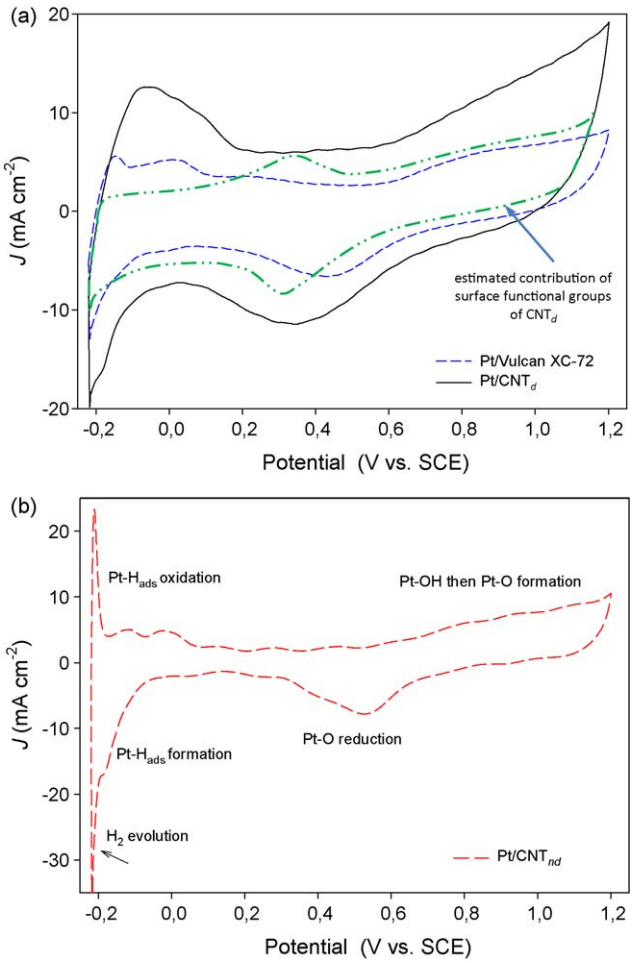

Fig. 7. Cyclic voltammetry (CV) curves of Pt/CNT_d (a) and Pt/CNT_{nd} (b). As reference, the CV curve for E-TEK Pt/Vulcan XC-72 sample is given. In Fig. 7a, the estimated contribution of surface functional groups of CNT_d on the CV curve of Pt/CNT_d is reported.

Pt–O reduction in Pt/CNT_{nd} may be recalculated to occur at about 0.40–0.45 V. There is thus anyway a shift to lower potential. Cherstiouk et al. [33] observed at shift of about 0.2 V in Pt–O reduction peak in passing from Pt nanoparticles with mean dimension of 7.5 nm (deposited on GC electrode) to Pt nanoparticles with mean dimension 1.5 nm (on defective pyrolitic carbon), attributed to a stronger adsorption of oxygen on the smaller particles. Similar observations were made also from Takasu et al. [34]. Looking in a more detail to the Pt–O reduction peak of Pt/CNT_{nd} (Fig. 7b), it may be observed that it is composed of two components, one centred at about 0.42 V and one centred at 0.55 V. This is consisted with the presence of a bimodial distribution of Pt nanoparticles in this sample (Fig. 6).

In the $Pt–H_{ads}$ oxidation region, three peaks could be observed in Pt/CNT_{nd}, at about −0.21 V vs. Ag/AgCl (the most intense and sharp), and at about −0.13 and −0.02 V. In Pt/CNT_d the first peak is absent and a broad peak centred near −0.08 V with a shoulder centred at +0.03 V could be noted. The latter is present also in the reference Pt/Vulcan sample, while the second peak is observed at −0.15 V. The different peaks are related to different crystalline exposed faces of Pt, but the size of nanoparticles and the interaction with the support also influence the position. Frequently, these peaks are simply identified as weak and strongly adsorbed hydrogen [35]. However, a unique relationship between position of the peaks and predominantly exposed crystalline plane, or type of Pt nanoparticles cannot be derived from literature data, at least for electrodes based on Pt supported on nanotubes. We may thus limit discussion indicating the qualitative difference in the $Pt–H_{ads}$ region between Pt/CNT_d and Pt/CNT_{nd}, which underline the different characteristics of Pt nanoparticles in the two types of carbon nanotubes.

The area of the $Pt–H_{ads}$ formation region, corrected for estimated carbon support contribution and double layer charge, can be used to estimate the electrochemical active surface area (EAS). The results are summarized in Table 1. It may be noted that EAS is about 20–25% lower than the geometrical surface area (GSA), a result which is consistent with literature observations. Cai et al. [26], for example, found that the percentage of Pt utilization, i.e. the ratio between EAS and GAS (indicated from them as chemical surface area, CSA), is about 80%. Considering that it is reasonable to assume a contact angle about 130–150° (with respect to 180° for an ideal round-shaped Pt particles without interaction with a flat carbon surface), from simple geometrical considerations it is possible to estimate that at least 20% of the ideal geometrical surface of Pt nanoparticle is not accessible to hydrogen adsorption. The data on EAS thus indicate that nearly all the Pt nanoparticles are accessible to hydrogen adsorption and electrochemical reaction. Based on EAS determination, the activity of Pt/CNT_d should be about 30% higher than that of Pt/CNT_{nd}.

3.3. Efficiency of three-phase boundary

CV experiments are often used to determine the electrochemical performances of electrodes, but we may observe that the performances in PEM fuel cells depend not only from the electroactive surface, but also from the possibility to realize an efficient three-phase boundary between the gas reactants, the proton diffusing to and from the membrane (at anode or cathode side, respectively), the metal nanoparticle, and the conductive carbon substrate for the flow of electrons. An efficient contact between the Nafion membrane and the catalyst layer, in particular, is a critical factor, which determines the overall performances. The contact at the Pt nanoparticle level, under standard (optimized) conditions of preparations, depends also on the wettability of the carbon nanotube from the Nafion, a sulfonated tetrafluoroethylene based fluoropolymer-copolymer. A better wettability, which in turns depends on the characteristics of the nanotube and thus also from its defective characteristics, allows a closer contact and thus a faster transport of protons to or from the noble metal nanoparticle.

Fig. 8 shows scanning electron microscopy (SEM) images of the interface between the Nafion membrane and the catalyst layer in Pt/CNT_d sample. The MEA is constituted from a carbon cloth (CC) substrate, necessary for allowing a good gas transport and for collecting the electrons, on which the Pt/CNT are deposited. The Pt/CNT/CC is then hot-pressed with the Nafion® 115 membrane to prepare the MEA. Fig. 8a and b shows the interface between the CC and Nafion at two magnifications, which indicate the good contact between the catalyst layer and the membrane. At higher magnification, the detail of the CNT deposited on the CC could be evidenced (Fig. 8c). EDX of a zone of this image (Fig. 8d) allows to estimate the effective contact between the Pt particles on the CNT and the Nafion from the ratio between the intensities of the EDX peaks of F (related to Nafion) and of Pt. The average between measurements in different zones (about 20) should be made for a better estimation. The results are summarized in Table 1. It may be observed that this ratio is about 40% higher in Pt/CNT_d with respect to Pt/CNT_{nd}, reasonably because the presence of a higher number of defects and associated functional groups in the former allows a better contact with the Nafion.

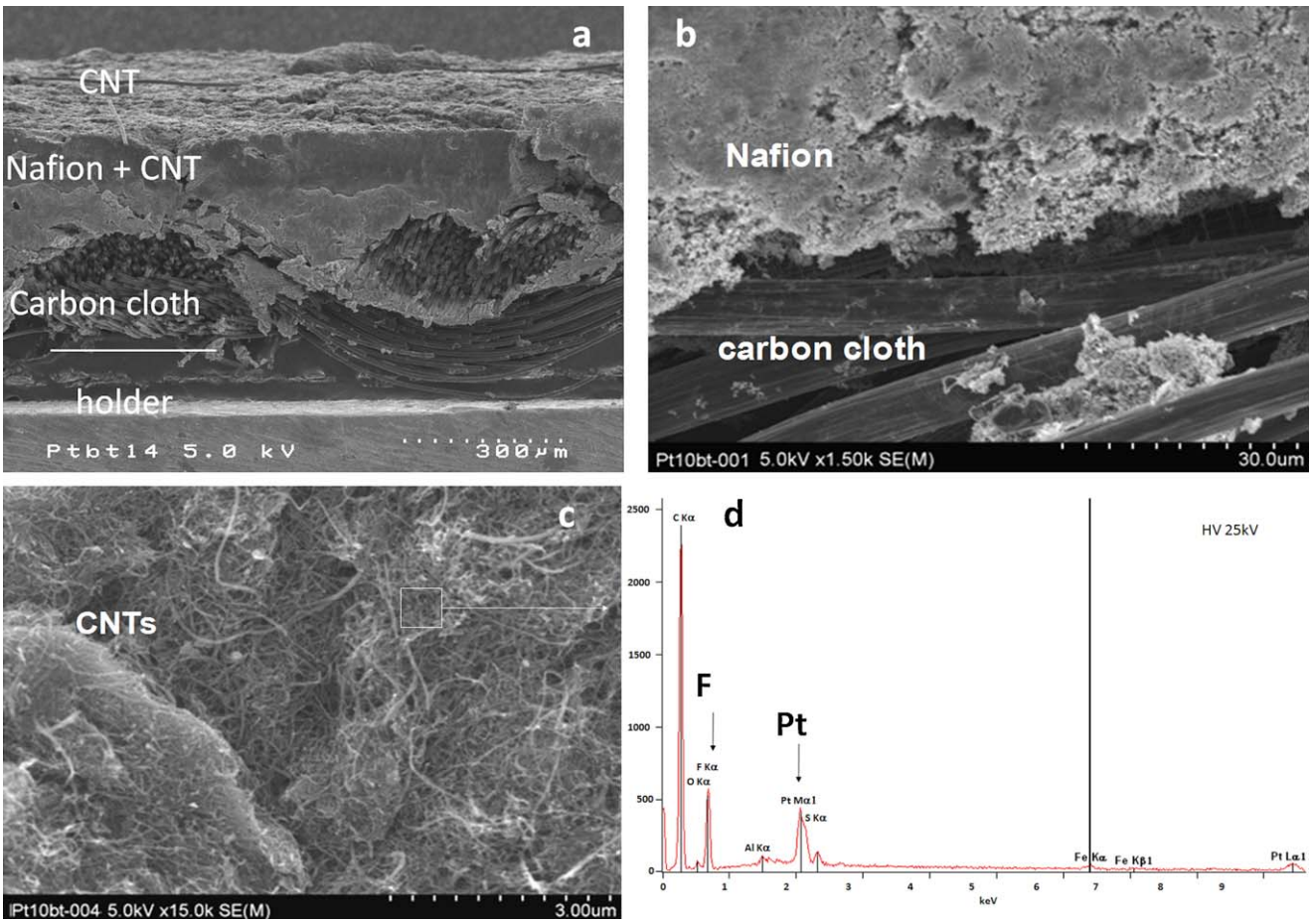

Fig. 8. (a–c) Scanning electron microscopy (SEM) images of Pt/CNT_d/CC/Nafion composite. (d) Energy-dispersive X-ray analysis (EDX) of the selected area.

3.4. Single-cell performances

Fig. 9 shows the single-cell performance for the MEAs made with Pt/CNT_d or CNT_{nd}/carbon paper composite electrode as anode (about 0.4 $mg_{Pt}\,cm^{-2}$) and standard E-TEK electrode (0.5 $mg_{Pt}\,cm^{-2}$) as cathode. Polarization curves were recorded at ambient temperature (about 20 °C) instead that at a temperature of around 80 °C as usual, because the objective was the analysis of the role of mechanically induced defects in the modifications of the properties of supported Pt nanoparticles, and not to maximize the performances. Therefore, reaction conditions to minimize other effects (limitation at cathode side and by mass-transfer) have been chosen. In order to have a better reference for the single-cell tests in the used reaction conditions, the performances of a MEA made using the E-TEK electrode (0.5 $mg_{Pt}\,cm^{-2}$) both at anode and cathode sides is also reported in Fig. 9a. This sample is indicated as E-TEK Pt/Vulcan XC-72.

Both Pt/CNT samples show better performances than this reference sample in the specific reaction conditions utilized for the single-cell tests, reasonably due to the presence in both samples of smaller Pt nanoparticles with respect to Pt/Vulcan XC-72. However, a significant difference between the two Pt/CNT samples could be also observed. By converting the polarization curves (Fig. 9a) to power density curves (Fig. 9b), it may be observed that the maximum power density is shown at approximately the same cell voltage (around 0.3 V), but the value is about 65% higher for Pt/CNT_d with respect to Pt/CNT_{nd}. The increase in the maximum power density is significantly larger than that expected from the differences in the electrochemical surface area (Table 1), indicating that additional effects are present.

In order to have further insight on this phenomenon, the data were analyzed in terms of modified Tafel equation [27,36], which were originally introduced for the cathode side, although are used here for the anode side:

$$E = E^{o} - b\log i - iR \tag{5}$$

where E is the cell potential, i the current density, b the so-called Tafel slope, and R is predominantly the ohmic resistance in the electrode and electrolyte responsible for the linear variation of potential vs. current density plot. E^{o} is related to the exchange current density i^{o} through the following equation:

$$E^{o} = E_r + b\log i^{o} \tag{6}$$

where E_r is the reversible potential for the anode reaction.

The experimental data were fitted to Eq. (5) by a non-linear least-square method in order to evaluate the kinetic parameters from regression analysis. The resulting values are given in Table 2, while Fig. 9c shows the good fitting of the data. It may be observed that the value of E^{o} is quite close for the two Pt/CNT samples, indicating that the exchange current (i^{o}), which is related to the reaction kinetics, is nearly the same. The value of R is about 25% higher for the Pt/CNT_{nd} with respect to Pt/CNT_d (Table 2). R is related to the ohmic resistance and depends on many parameters. However, all conditions of preparation are the same, apart the nature of CNT. The differences observed for the single-cell performances are reproducible when the samples are prepared again and thus may be reasonable to assume that the difference in R value is related to the different electronic conduction of the CNT.

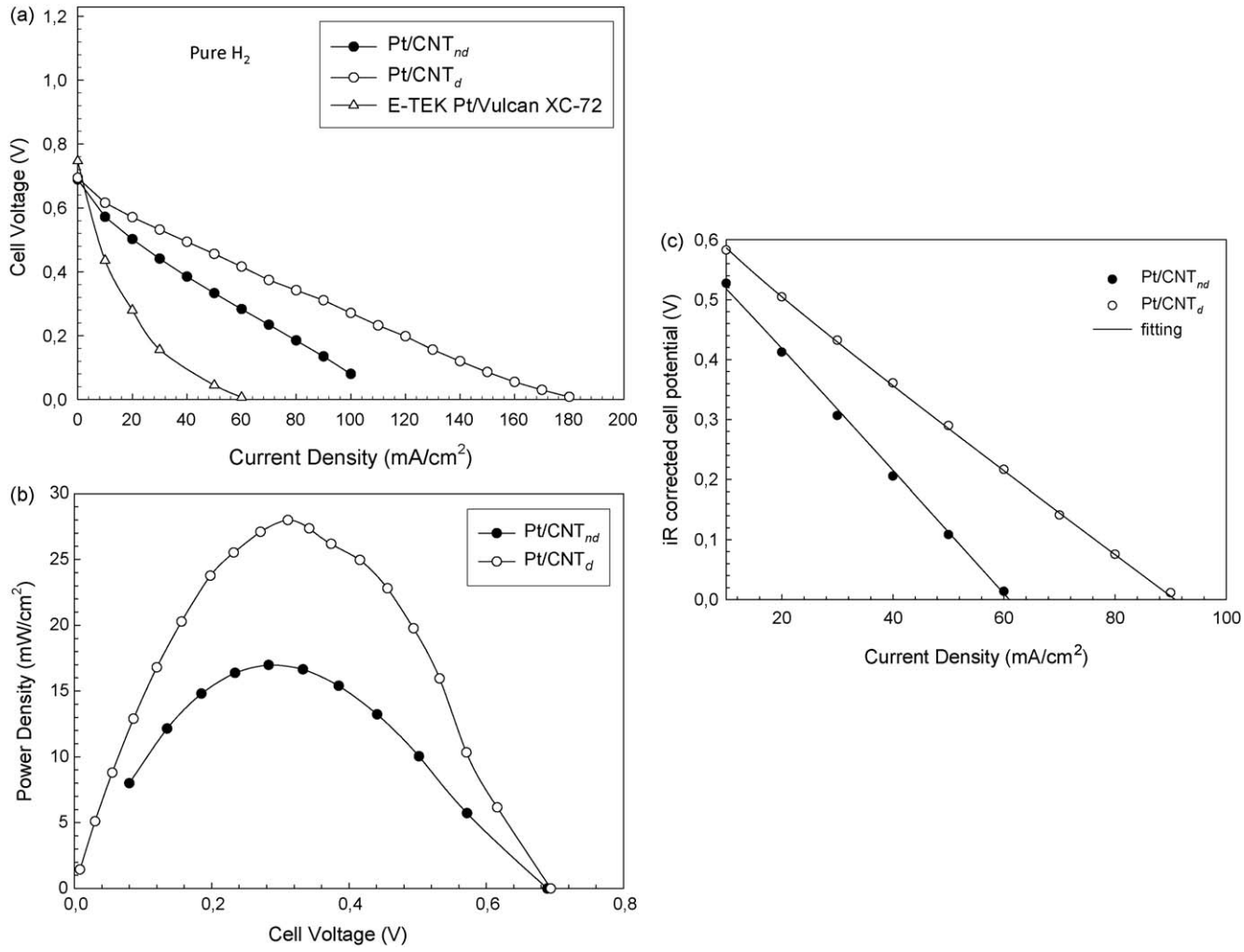

Fig. 9. Single-cell tests. Polarization (a) and power density curves (b) obtained using as anode MEA (membrane-electrode assembly) based on Pt/CNT_d and Pt/CNT_{nd} deposited on carbon cloth (CC). Fig. 9c reports the *iR* corrected cell potential vs. current density and the fitting obtained using Eq. (5) and the parameters reported in Table 2. E-TEK Pt/Vulcan XC-72 on CC was used as cathode to which oxygen saturated with H_2O at r.t. was feed. Nafion® 115 was used as membrane. As reference, the polarization curve of a MEA based on E-TEK Pt/Vulcan XC-72 on CC electrode on both sides is shown. Reaction conditions: room temperature (20 °C), 1 atm, feed of pure H_2 (saturated at r.t. with H_2O) at the anode side.

A larger difference is also observed in the value of the Tafel slope (b) (Table 2). This parameter is related to the mechanism of activation of H_2, which in turns depends on the characteristics of the Pt nanoparticles and the nature of the interaction with the carbon substrate. The result is consistent with the TEM data and CV results discussed before.

Therefore, the nature of CNT and the presence of defects influence many aspects, not only the dispersion of Pt and the related electrochemically active surface. There is an influence on the (i) efficiency of the contact with Nafion and thus on the proton transfer and effectiveness of three-phase boundary, as commented in the previous Section 3.3, (ii) resistance of electron transfer, as indicated from the different value of *R* parameter in Table 2, and (iii) specific characteristics of Pt particles, not only in terms of dispersion, but also in terms of carbon substrate–metal particle interaction which reasonably influences the specific characteristics and reactivities of the supported Pt particles.

Table 2
Parameter estimated by non-linear fitting of Eq. (5) for polarization curves obtained at r.t. in single-cell tests using pure H_2 at the anode.

Sample	E^o (V)	b (V^{-1})	R (V/mA)
Pt/CNT_d	7.035e−1	2.186e−2	3.329e−3
Pt/CNT_{nd}	6.989e−1	3.580e−2	4.490e−3

For this reason, the performances in single-cell tests cannot be correlated only to the electrochemical active surface area (EAS), and to the role of CNT in favoring the dispersion of the supported noble metal, as often reported in literature. Other aspects related also to CNT characteristics are important, such as the CNT electronic conductivity and effectiveness of contact with Nafion. Although at higher temperature these effects may be masked from other aspects which are typically considered the only limiting factors determining the cell performances, such as oxygen reduction and mass transport, it is reasonable to consider that they still play a role and that part of the contradicting literature data could be related from a scarce consideration of above aspects.

3.5. Single-cell tests in the presence of CO

In Pt/CNT_d smaller and uniform in size Pt nanoparticles are present with respect to Pt/CNT_{nd} where a bimodial and broader distribution of Pt nanoparticles is present (Fig. 6). It is known that different crystalline planes could be stabilized as a function of the nanoparticle size. CV curves confirm the presence of different type of $Pt–H_{ads}$ species in the two samples. Therefore, the non-linear

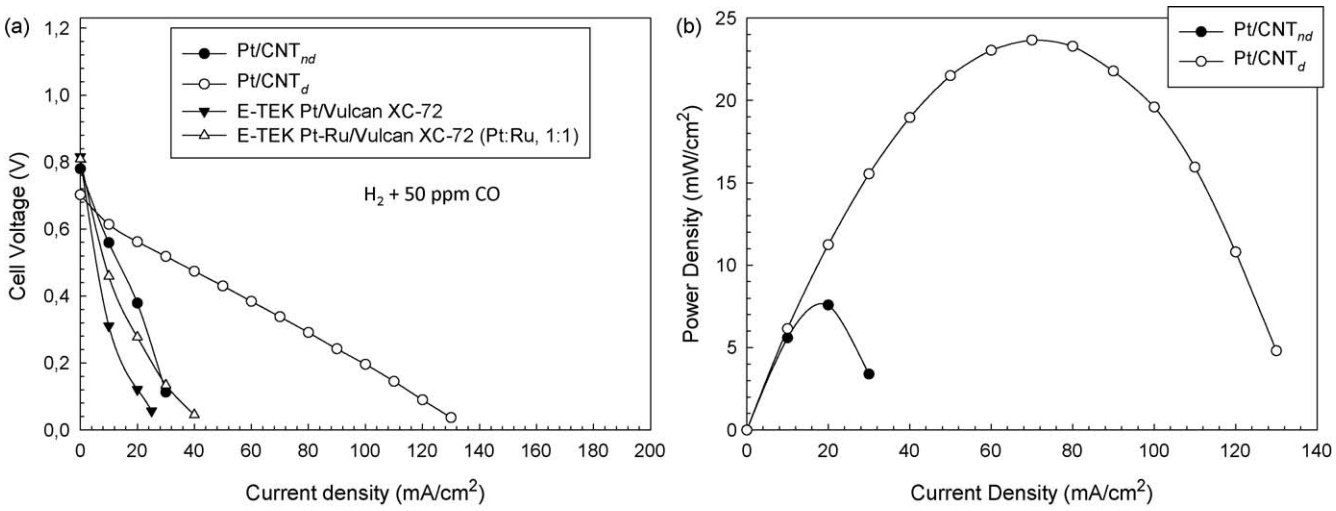

Fig. 10. Single-cell tests. Polarization (a) and power density curves (b) obtained using as anode MEA (membrane-electrode assembly) based on Pt/CNT$_d$ and Pt/CNT$_{nd}$ deposited on carbon cloth (CC). Other conditions as in Fig. 9, except that the H_2 feed at anode side contains 50 ppm CO. As reference, the polarization curves of a MEA based on E-TEK Pt/Vulcan XC-72/CC or Pt–Ru (1:1)/Vulcan XC-72/CC anode and E-TEK Pt/Vulcan XC-72/CC cathode are shown.

relation between EAS and single-cell performances could be related to this aspect. It is known that the hydrogen reaction is a structure sensitive process, with Pt(1 1 0) being an order of magnitude more active than either of the atomically "flatter" (1 0 0) end (1 1 1) surfaces. However, it has been observed by in situ techniques that a reconstruction of the metal particles occurs during fuel cell operations [37]. Recent in situ X-ray absorption fine structure (XAFS) measurements of Pt supported on Vulcan XC-72 operating as a cathode catalyst in a polymer electrolyte membrane fuel cell evidenced changes in the near-edge structures reflecting variations in the Pt electronic structure, which were a function of the potential values [38]. It is reasonable to expect a fast dynamic of reconstruction during operations, due to the higher charge to volume ratio in the smaller Pt nanoparticles during fuel cell operations. Therefore, particularly for the small nanoparticles (<2 nm) present in Pt/CNT$_d$ sample, may be questionable to attribute the enhanced performances to the presence of a more active crystalline plane such as Pt(1 1 1), if there is a dynamic reconstruction of the particles during operations.

On the other hand, smaller nanoparticles have a higher relative amount of perimetral sites at the contact with the carbon. If these sites play a role in the electrocatalytic mechanism, smaller nanoparticles should have a higher specific activity per unit of metal surface area.

In order to try to understand this aspect and to analyze a further role of defects in CNT, the single-cell performances of Pt/CNT samples in the presence of CO were evaluated. The presence of structure sensitivity in the poisoning effect of CO in electro-oxidation of H_2 is still unclear. While several authors consider the presence of this effect [39], other authors found different results. Atalika and Uner [40] observed that the dispersion and particle size of Pt has a minimal effect on CO oxidation in the presence of large amounts of H_2. Uchida et al. [41] do not observed a particle-size effect on the hydrogen oxidation reaction with and without CO poisoning. On the other hand, it was known that the CO-tolerance of Pt–Ru electrocatalysts is related to the formation of Brönsted acid sites (due to water activation) that catalyze the oxidation of CO [42,43]. CV tests (Fig. 7a) have evidenced the higher presence of surface functional oxygen-containing groups on CNT$_d$, which reasonably act also as anchoring sites for the Pt nanoparticles. These sites could assist in CO oxidation and thus improve the CO-tolerance of the electrocatalysts, particularly when very small Pt nanoparticles (<2 nm) are present as in out Pt/CNT samples.

Reported in Fig. 10a are the polarization curves for Pt/CNT$_{nd}$ and Pt/CNT$_d$ samples in the presence of 50 ppm CO in the H_2 feed and in Fig. 10b the relative curves of power vs. current density. Also these tests have been made at room temperature and for this reason, for a better comparison, the performance of a reference E-TEK Pt/Vulcan XC-72 has been reported. Being usually utilized Pt–Ru bimetallic particles to improve the tolerance to CO deactivation, the behaviour of a reference E-TEK Pt–Ru/Vulcan XC-72 (Pt:Ru = 1:1) has been also reported. Although the behaviour is slightly better than that of the Pt-only E-TEK sample, the improvement is limited. This is due to the low temperature of these tests, where the effect of Ru, related to the ability of forming Ru–OH sites by water electroactivation which promote the oxidation of CO to CO_2 [42,43], in not effective. The behaviour of Pt/CNT$_{nd}$ is quite similar to that of these two E-TEK reference samples, with a maximum power density of about 8 mW cm^{-2}, i.e. a decrease of more than 50% with respect to the performance in pure H_2 (Fig. 9b) in the same conditions. The deactivation effect of CO on the power density of Pt/CNT$_d$ was instead observed to be much less relevant. The maximum value decreases from about 28–24 mW cm^{-2} in adding 50 ppm CO to the H_2 feed, i.e. a decrease of less than 15%. The Pt/CNT$_d$ shows thus a CO-tolerant behaviour even at room temperature and in the absence of other metals, reasonably due to the presence of very small Pt nanoparticles in close contact with defective sites of the carbon nanotube.

To analyze more in detail these aspects, it is worth to analyze whether the maximum power density (MPD) correlates only with the presence of small Pt nanoparticles in Pt/CNT samples. Using the experimental distribution of Pt particles (Fig. 6) it is possible to calculate the fraction of the total surface area deriving from the particles below a critical size (1.5 nm for example) and then estimate the electrochemical active surface area (EAS) of these particles by multiplying this fraction for the total measured EAS (Table 1). This EAS for particles below 1.5 nm may be then put in relation with the MPD value for single-cell tests with or without the presence of CO in the H_2 flow. The results are summarized in Fig. 11.

It may be noted that assuming active only the particles with size ≤1.5 nm, a linear relationship could be observed in the case of H_2, but not when CO is present in the feed. This further evidence that it is not present only a role of CNT in determining the dispersion of supported Pt particles, but there are additional effects, as commented above. In particular, it is suggested that the presence

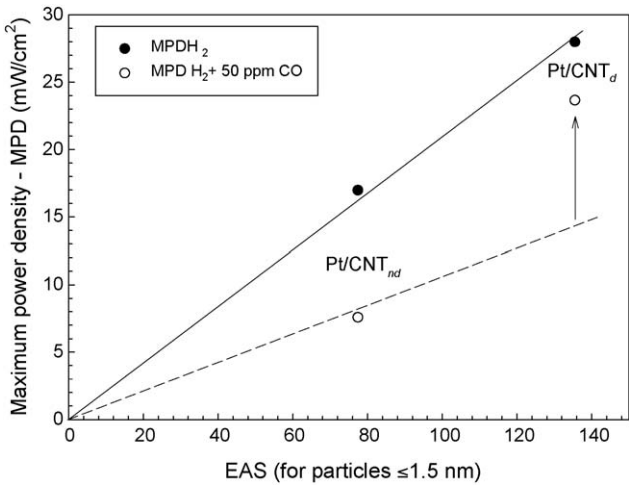

Fig. 11. Relation between electrochemical active surface area (EAS) for particles ≤1.5 nm (see text) and maximum power density (MPD) for single-cell experiments using pure H_2 or H_2 plus 50 ppm CO feeds at the anode side. Reactions conditions for MPD indicated in Fig. 9.

of mechanically induced defects in the CNT could be relevant to stabilize very small Pt nanoparticles and improve tolerance by CO deactivation.

4. Conclusions

The analysis of the characteristics and reactivity of two anodes based on Pt supported on carbon nanotubes (CNTs) without or with defects induced by ball-milling evidences that the presence of defects influences several properties and not only the dispersion of Pt particles, as often assumed. Therefore, the performances cannot be correlated neither with the geometrical surface area of Pt particles, neither with the electrochemical active surface area determined from CV tests. The presence of defects, enhancing the amount of surface functional groups on CNT, influences various aspects:

(i) the efficiency of three-phase boundary and thus the transport of protons to or from the active metal particles,
(ii) the resistance of electron transfer,
(iii) the tolerance of the catalyst to CO poisoning.

The latter is attributed to carbon functional groups in close contact with very small Pt particles favoring the reactivation of Pt sites poisoned by CO. It was also observed that assuming active only the particles with size ≤1.5 nm, a linear relationship could be observed in the case of pure H_2 feedstock to the anode, but not when CO is also present in the feed. This further evidence that it is not present only a role of CNT in determining the dispersion of supported Pt particles, but there are additional effects, as commented above. These data suggest that the presence of mechanically induced defects in the CNT could be relevant to stabilize very small Pt nanoparticles and improve tolerance by CO deactivation.

The results also indicate that the performances in single-cell tests cannot be correlated only to the electrochemical active surface area (EAS), and to the role of CNT in favoring the dispersion of the supported noble metal, as often reported in literature. Other aspects related also to CNT characteristics are important, such as the CNT electronic conductivity and effectiveness of contact with Nafion. Even if at higher temperature these effects may be masked from other aspects which are typically considered the only limiting factors determining the cell performances, such as oxygen reduction and mass transport, it is reasonable to consider that they still play a role and that part of the contradicting literature data could be related from a scarce consideration of above aspects.

Although these results should be further proven with more extensive studies on the relationship between properties of CNT and performances of Pt/CNT based electrodes for PEM fuel cells, they evidence the higher complexity of the phenomena in analyzing the use of carbon nanotubes for preparing improved electrodes and suggest that specific attention should be given to the role of defects.

It should be commented, however, that this study was centred on the behaviour of the anode of PEM fuel cells, while usually is stated that the cathodic reaction (not the anodic reaction) is the limiting reaction under all conditions (pure oxygen or air, low and high T, etc.). Even if the reaction at the cathode is the slower one in semi-cell tests, the concept of kinetic rate-limiting step cannot be applied in full-cell tests, where the cathode and anode sides are electronically/ionic connected, because the system is in a quasi-thermodynamic equilibrium. The concept of kinetic rate-limiting step at the cathode side implies that the modification of anode side should be not effective, because it is already faster than at the cathode side. However, the experimental data in our case (Fig. 9) evidence that the properties of the electrocatalyst at the anode side considerably influence the performances. In addition, the deactivation effect of CO also evidences that the reaction at the anode side determines the overall performances. We may thus conclude that at least in the experimental conditions used in this work the characteristics of the electrocatalyst at the anode side determine the overall behaviour and the correlation between electrocatalyst properties and cell performances may be thus analyzed.

In fact, it was necessary to investigate the anode side, in order to analyze in a more complete way the effect of defects in carbon nanotubes, e.g. to include also the effect of the deactivation by CO. However, we have operated at lower temperature (r.t.) than the usual one utilized in PEM fuel cells (about 70 °C), in order to avoid mass-transfer limitations. These limitations should be taken into account in analysing this work and relative conclusions.

Acknowledgements

The authors would like to acknowledge the European commission for its financial support in the NEST programme "ELCAT", Professor Sylvie BEGIN for ball-milling experiments and Dr. Daniele Cosio for the precious technical assistance.

References

[1] Y. Shao, J. Liu, Y. Wang, Y. Lin, J. Mater. Chem. 19 (1) (2009) 46.
[2] J. Liu, G. Cao, Z. Yang, D. Wang, D. Dubois, X. Zhou, G.L. Graff, L.R. Pederson, J.-G. Zhang, ChemSusChem 1 (2008) 676.
[3] Y.-G. Guo, J.-S. Hu, L.-J. Wan, Adv. Mater. 20 (2008) 2878.
[4] A.L. Dicks, J. Power Sources 156 (2006) 128.
[5] K. Lee, J. Zhang, H. Wang, D.P. Wilkinson, J. Appl. Electrochem. 36 (5) (2006) 507.
[6] M. Gangeri, G. Centi, A. La Malfa, S. Perathoner, R. Vieira, C. Pham-Huu, M.J. Ledoux, Catal. Today 102–103 (2005) 50.
[7] M. Gangeri, S. Perathoner, G. Centi, Inorg. Chim. Acta 359 (2006) 4828.
[8] M.S. Saha, R. Li, X. Sun, S. Ye, Electrochem. Commun. 11 (2) (2009) 438.
[9] Z. Cui, C. Liu, J. Liao, W. Xing, Electrochim. Acta 53 (27) (2008) 7807.
[10] T. Maiyalagan, Appl. Catal. B: Environ. 80 (3–4) (2008) 286.
[11] H. Kim, N.J. Jeong, S.J. Lee, K.S. Song, Korean J. Chem. Eng. 25 (3) (2008) 443.
[12] E.K. Tuseeva, N.A. Mayorova, V.E. Sosenkin, N.F. Nikol'skaya, Yu.M. Vol'fkovich, A.V. Krestinin, G.I. Zvereva, V.A. Grinberg, O.A. Khazova, Russ. J. Electrochem. 44 (8) (2008) 884.
[13] Y. Verde, R. Gomez-Vargas, G. Gonzalez, W. Antunez, G. Alonso, ECS Trans. 3(1, Proton Exchange Membrane Fuel Cells 6) (2006) 313.
[14] G. Wu, B.Q. Xu, J. Power Sources 174 (2007) 148.
[15] W.Z. Li, X. Wang, Z.W. Chen, M. Waje, Y.S. Yan, J. Phys Chem. B 110 (2006) 15353.
[16] S. Shanmugam, A. Gedanken, Electrochem. Commun. 8 (2006) 1099.
[17] Y.Y. Shao, G.P. Yin, J. Zhang, Y.Z. Gao, Electrochim. Acta 51 (2006) 5853.
[18] L. Gan, R. Lv, H. Du, B. Li, F. Kang, Electrochem. Commun. 11 (2) (2009) 355.
[19] J.-G. Wang, Y.-A. Lv, X.-N. Li, M. Dong, J. Phys. Chem. C 113 (3) (2009) 890.
[20] E. Yoo, T. Okada, T. Kizuka, J. Nakamura, J. Power Sources 180 (1) (2008) 221.

[21] C. Xu, J. Chen, Y. Cui, Q. Han, H. Choo, P.K. Liaw, D. Wu, Adv. Eng. Mater. 8 (1–2) (2006) 73.
[22] Z. Osváth, G. Vértesy, L. Tapasztó, F. Wéber, Z.E. Horváth, J. Gyulai, L.P. Biró, Phys. Rev. B 72 (2005) 045429.
[23] J.-H. Ahn, H.-S. Shin, Y.-J. Kim, H. Chung, J. Alloys Compd. 434–435 (2007) 428.
[24] E. Yoo, T. Okada, T. Kizuka, J. Nakamura, Electrochemistry (Tokyo, Japan) 75 (2) (2007) 146.
[25] T.J. Schmidt, H.A. Gasterger, G.D. Stab, P.M. Urban, D.M. Kolb, R.J. Behm, J. Electrochem. Soc. 145 (1998) 2354.
[26] K.-D. Cai, G.-P. Yin, J.-J. Wang, K.-L. Lu, Energy Fuels 23 (2009) 903.
[27] M.S. Saha, R. Li, X. Sun, J. Power Sources 7 (2008) 314.
[28] R.N. Carter, S.S. Kocha, F.T. Wager, M. Fay, H.A. Gasteiger, ECS Trans. 11 (1) (2007) 403.
[29] A. Pozio, M.D. Francesco, A. Cemmi, F. Cardellini, I. Giorgi, J. Power Sources 105 (2002) 13.
[30] F. Maillard, M. Martin, F. Gloaguen, J.M. Leger, Electrochim. Acta 47 (2002) 431.
[31] Y.B. Li, B.Q. Wei, J. Liang, Q. Yu, D.H. Wu, Carbon 37 (1999) 493.
[32] J. Maruyama, I. Abe, Electrochim. Acta 46 (2001) 3381.
[33] O.V. Cherstiouk, P.A. Simonov, E.R. Savinova, Electrochim. Acta 48 (2003) 3851.
[34] Y. Takasu, N. Ohashi, X.-G. Zhang, Y. Murakami, H. Minigawa, S. Sato, K. Yahikozawa, Electrochim. Acta 41 (1996) 2595.
[35] I. Avila, M. Garcia, M.A. Plata-Torres, C. Domingues-Crespo, E.M. Ramirez-Rodriguez, Arce-Estrada, J. Alloys Compd. 434–435 (2007) 764.
[36] E.A. Ticianelli, C.R. Derouin, A. Redondo, S. Srinivasan, J. Electrochem. Soc. 135 (1988) 2209.
[37] S. Stoupin, E.-H. Chung, S. Chattopadhyay, C.U. Segre, E.S. Smotkin, J. Phys. Chem. B 110 (2006) 9932.
[38] A. Witkowska, E. Principi, A. Di Cicco, S. Dsoke, R. Marassi, L. Olivi, M. Centazzo, V.R. Albertini, J. Non-Crystal. Solids 354 (35–39) (2008) 4227.
[39] K.J.J. Mayrhofer, M. Arenza, B.B. Blizanac, V. Stamenkovic, P.N. Ross, N.M. Markovic, Electrochim. Acta 50 (2005) 5144.
[40] B. Atalika, D. Uner, J. Catal. 241 (2) (2006) 268.
[41] H. Uchida, K. Izumi, M. Watanabe, ECS Trans., 11(1, Part 2, Proton Exchange Membrane Fuel Cells 7, Part 2) (2007) 913.
[42] X. Cheng, Z. Shi, N. Glass, L. Zhang, J. Zhang, D. Song, Z.-S. Liu, H. Wang, J. Shen, J. Power Sources 165 (2) (2007) 73.
[43] T.R. Ralph, M.P. Hogarth, Platinum Metals Rev. 46 (3) (2002) 117.